Sixth International Symposium on Turbulence and Shear Flow Phenomena
Seoul, Korea, 22-24 June 2009

STATISTICAL MODELING OF VORTEX GENERATORS IN PRESSURE GRADIENT BOUNDARY LAYERS

Florian von Stillfried[a]
Stefan Wallin[a,b], **Arne V. Johansson**[a]
[a] Royal Institute of Technology Stockholm
Linné Flow Centre
Department of Mechanics
100 44 Stockholm, Sweden

[b] Swedish Defence Research Agency
Computational Physics
164 90 Stockholm, Sweden

florian@mech.kth.se, stefan.wallin@foi.se, viktor@mech.kth.se

ABSTRACT

Modeling arrays of passive vortex generators (VGs) pairs, mounted in a flat plate boundary layer with adverse pressure gradient (APG) flow and generating streamwise counter rotating vortex structures is the object of this investigation. Usually, a sound computational fluid dynamics (CFD) investigation requires an adequate grid with a corresponding large number of grid points around such VGs in order to obtain an accurate solution of this flow case. This, in turn, leads to a time-demanding grid generation which often comes along with lots of practical challenges during the creation. An effective way to get around this time-consuming process is to introduce a way to model these flow separation devices statistically and, by that, to add their statistical physical effects to the governing equations rather than resolving their geometries in the computational grid. This approach for the modeling of passive VGs turbulent flow separation devices is presented for APG flow over a flat plate using the CFD code Edge by FOI, the Swedish Defence Research Agency. Moreover, computational results for three dimensional fully resolved VGs as well as experimental results without VGs are evaluated and compared to this statistical VG model approach. It is shown that flow separation can be successfully prevented by means of the statistical VG model.

INTRODUCTION

The operational envelope in aeronautical and other engineering designs is in many cases limited by turbulent boundary layer separation. The possibility of controlling and delaying the separation enables more efficient designs that can be used for improving the performance or for optimizing the design in order to reduce drag and weight. Turbulent boundary layers can be energized by introducing vortices by vortex generators (VGs) that increase the mixing of momentum in the boundary layer and, by that, increase the near-wall velocity. Experimental studies as well as computations have shown the ability of controlling separation with such devices. Lin (2002) provides a review of the research activities in the field of passive low profile vortex generators (LPVGs). Basic fluid dynamics and applied aerodynamics research of the performance enhancement of various flow cases due to LPVGs is presented. LPVGs are most efficient when flow separation is relatively fixed and they produce "minimal near-wall protuberances" in order to overcome flow separation. The height of such LPVGs is typically around $0.1 \leq h/\delta_{99} \leq 0.5$ which in turn reduces drag compared to larger VGs but still ensures the LPVGs acting as highly effective control devices against flow separation compared to conventional designs.

In computational fluid dynamics (CFD), the most straightforward way to mimic VGs is to fully resolve their geometry within the mesh. This leads to very fine mesh spacings in the vicinity of such VG structures in order to resolve the developing boundary layer on the VG vane surface as well as the developing vortex structures in its vicinity and further downstream. Thus, fully resolved VGs lead to high computational costs. A statistical VG model approach was introduced by Törnblom and Johansson (2008). This model approach describes the statistical effects of VGs on the flow. Here, the vortex flow field is derived by only taking the geometrical properties of VGs into account, inspired by Wendt (2001). The circulation distribution $\Gamma(y)$ across one VG blade is needed as an input for the VG modeling and is estimated by the lifting line theory (LTT), see e.g. Glauert (1926), or Anderson (1991). Then, the resulting cross stream vortex velocity field is added indirectly by means of the second order statistics of the generated vortex velocity field in a small region through forcing terms in a Reynolds stress transport (RST) model. Furthermore, the drag generation of the modeled VGs is considered by added volume forces in the streamwise component of the momentum equation. An advantage of this method is that no mesh refinement is needed and that the computational costs compare solely with solving the Reynolds averaged Navier-Stokes (RANS) equations, thus, enabling design and optimization of VG settings by CFD.

Investigations of this statistical VG model in a zero pressure gradient (ZPG) boundary layer flow over a flat plate are presented in von Stillfried et al. (2009). There, the VG model could be successfully applied to the ZPG flow case and the investigation has shown that the statistical modeling of VGs was effectually deployed and has the advantage of not being more computational expensive than solving RANS equations.

The main objective of this work is to examine the capabilities of the statistical VG model in adverse pressure gradient (APG) flow over a flow plate. First, the clean flat

plate with APG was investigated and adjusted in order to match experimental results, i.e. the wall pressure distribution along the streamwise coordinate. Then, the two dimensional (2D) VG model was introduced in the flow at the respective position as in experiments. Second, a parameter variation study was conducted, using different streamwise positions for the VG model forcing region. The results were then compared to experimental results without flow control devices and to three dimensional (3D) computations including fully resolved VGs.

ANALYTICAL AND NUMERICAL METHODS

The modeling of the VGs in this investigation follows the way suggested by Törnblom and Johansson (2008) who presented a model that requires neither mesh refinements nor 3D computations. In this model approach, the VGs are represented by a vortex source model that uses the lifting line theory in order to estimate the generation of circulation by the VGs. The circulation distribution Γ(y) across a wing according to the LLT is given by

$$\Gamma(y) = \frac{K}{2} U(y) c(y) \left[\alpha(y) - \frac{w(y)}{U(y)} \right] \tag{1}$$

where K is the local section lift slope of the wing (K_{max} $= 2\pi$ rad^{-1} according to thin airfoil theory[1]), U(y) is the local incoming free stream velocity, c(y) the local chord length of the wing, α(y) the local angle of attack, and w(y) the local downwash due to the trailing vortex sheets. The ratio w(y)/U(y) is the local induced angle of attack α_{ind}(y) for small angles α, and the local downwash w(y) reads

$$w(y) = \frac{1}{4\pi} \int_{-h}^{h} \frac{d\Gamma}{dy'} \frac{1}{y' - y} dy' \tag{2}$$

Equations (1) and (2) are solved by means of a Fourier series ansatz, see e.g. Anderson (1991). The LLT holds for high aspect ratio (AR) wings in free flight conditions for small angles of attack α far away from obstacles in the flow. By modeling VGs that are mounted on a wall in a boundary layer flow by means of the LLT, some of its original assumptions are not valid anymore as a result of:

1. a boundary layer velocity profile U(y) instead of a constant free stream velocity U_∞,
2. VGs being very low AR wings,
3. possible side effects due to the proximity of neighbouring VG blades, i.e. neighbouring vortices,
4. a reasonable high angle of incidence α (corresponding the angle of attack α for free flight in the LLT) of the VG blades.

Therefore, the LLT is only used as an approximation to estimate the circulation distribution Γ(y) across a single VG blade. In turn, the circulation distribution Γ(y) quantitatively describes the generated lift, the induced drag and the vortex strength which is again needed as an input for the vortex model. The vortices are then represented by a Lamb-Oseen vortex model with the azimuthal velocity distribution

$$u_\Phi(r) = \frac{\Gamma_{max}}{2\pi r} \left[1 - \exp\left(\frac{-r^2}{r_0^2} \right) \right] \tag{3}$$

where Γ_{max} is the maximum value of the circulation distribution Γ(y), determined from the LLT (see Eq. (1)), r_0 the vortex core radius and r the radial coordinate from the vortex center. A limitation of this 2D vortex model is that the velocity component in the streamwise direction is constant.

A VG array consists of more than one VG so that all VGs influence the vortex flow field everywhere in the VG plane[2]. Due to that, a superposition of the vortex induced velocities u_Φ(r) for each VG and their corresponding blades was needed. The wall acts approximately as a symmetry condition for the vortices, which is simulated by introducing mirror vortices.

The concept of this VG model approach and describing its effects on the flow is to assume that the second order statistics of the additional vortex velocity field act like additional Reynolds stresses on the mean flow. By making this assumption, the additional spanwise averaged contributions $\Delta\overline{u_i' u_j'}$(y) to the Reynolds stresses are

$$\Delta\overline{u_i' u_j'}(y) = \frac{1}{D} \int_{-D/2}^{D/2} u_i'(y,z) u_j'(y,z) dz \tag{4}$$

It is sufficient to integrate and spanwise average the second order statistics in Eq. (4) over one VG pair distance D since the resulting vortex flow field is periodic. Additional contributions from Eq. (4) are only nonzero for $\Delta\overline{v'v'}$ and $\Delta\overline{w'w'}$. Moreover, a wall damping function, e.g. (1-exp(-20y/h)), needed to be introduced and applied on Eq. (4) because the vortex velocities in the spanwise direction at the wall boundary y = 0 will not cancel out and would result in a finite value in Eq. (4).

After applying the additional stresses, a RST turbulence model was used to properly describe the development of the total Reynolds stresses downstream of the VG plane. Furthermore and unlike simpler turbulence models, a RST turbulence model makes it possible to account for the energy transfer between the different components of the Reynolds stress tensor, thus enabling production of $\overline{u'v'}$ Reynolds stresses.

EXPERIMENTAL SET-UP

The corresponding geometry of the modeled VGs was earlier experimentally examined by Lögdberg et al. (2009), see also figures 1, 2 and Table 1. Each VG pair consisted of two rectangular flat plates of height h = 18 mm, mounted at angles of incidence $\alpha = \pm 15°$, and a chord length c/cos α with c = 54 mm being the projected chord in the streamwise direction. The mean distance between such two blades was d = 37.5 mm and the distance between two adjacent VG pairs was D = 150 mm. The VGs were mounted in an array consisting of N = 5 VG pairs with their trailing edges (TE) located at $x_{VG_{TE}} = 1.54$ m from the leading edge (LE) of the flat plate in the test section of the BL wind tunnel at KTH Stockholm. The free stream velocity U_∞ was 26.5±0.1 m/s and the temperature had a constant value of 20°C. At that streamwise position, the boundary layer thickness had a value of $\delta_{99} = 42$ mm and, therefore, the VGs can be characterized as LPVGs, giving a ratio $h/\delta_{99} = 0.43$. The BL wind tunnel has a 4.0 m long test section with a cross sectional area of 0.75 x 0.50 m^2 and features a temperature control system for keeping a constant temperature within

[1] The unit rad^{-1} will generally be neglected when K is mentioned in the rest of this paper

[2] Throughout this paper, the VG plane is assumed to be the corresponding yz-plane at the streamwise trailing edge location of the experimental VG blades.

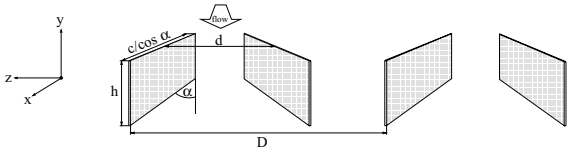

Figure 1: Vortex generator geometry from experiments, data given in table 1.

Table 1: Vortex generator geometry data from experiments.

h [m]	d [m]	D [m]	c [m]	α [°]	$x_{VG_{TE}}$ [m]
0.018	0.0375	0.150	0.054	±15	1.54

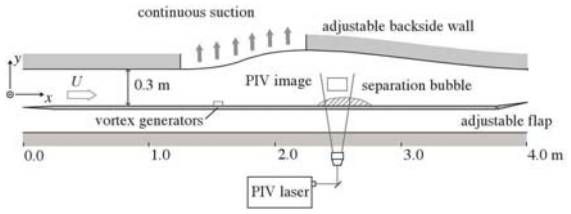

Figure 2: Sketch of the BL wind tunnel test section used in experiments, taken from Lögdberg et al. (2009).

± 0.03°C. A flat plate made of acrylic glas splits the wind tunnel's test section and is mounted with a distance of 0.30 m to the test section's upper wall, see Fig. 2. At the wind tunnel inlet, the test section has a width of 0.50 m which is diverged by a back side curved wall at 1.25 m downstream of the flat plate LE in order to induce the APG. Furthermore, a suction system is installed at the curved wall so that flow separation is prevented there. Another feature of the suction system was the additional capability to change the APG strength through adjusting the suction rate at the curved wall. In total, three different APG cases were performed with suction rates of $6-7$ %, $12.5-13$ % and 17 % of the incoming mass flow, see Fig. 2. All flow field measurements were performed with PIV. The interested reader is referred to Lindgren and Johansson (2004) for further details of the wind tunnel and to Lögdberg et al. (2009) as well as Angele (2003) for further details of the experiments, the set-up and the measurement techniques.

During this investigation, case II with a suction rate of $12.5-13$ % and its corresponding resulting pressure distribution was used for setting up the computations and for later comparison, see also Fig. 3 where all three different APG cases and their pressure coefficient distributions are shown. Case II represented the most comprehensive investigated APG case and was therefore chosen for this investigation. The separation bubble for the experiments was defined as the region where at least 50 % backflow at the wall is developed, i.e. the wall backflow coefficient $\chi_w \geq 0.5$. According to Dengel and Fernholz (1990), χ was extrapolated to the wall from the data points in the region y ≈ 1.5 - 10 mm in order to estimate χ_w. The resulting geometrical properties such as the separation location x_{sep}, the reattachment location x_{att}, the length l_{sep} as well as the height of the separation bubble h_{sep} are given in the first data row in table 2.

COMPUTATIONAL SET-UP

This investigation includes three computational cases:

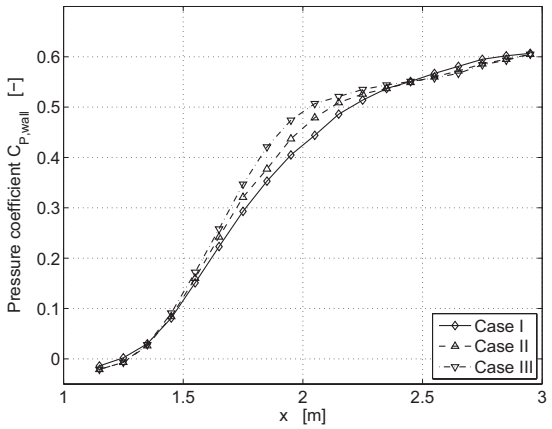

Figure 3: Wall pressure coefficient distribution for the three different experimental APG cases.

one 2D case of a clean flat plate, one 2D case with the VG model applied and a 3D case that fully resolved the VG vanes on the flat plate. The following abbreviations are used in this paper in order to label the different computations:

1. FP2D for the 2D flat plate without VG model,
2. VG2D for the 2D flat plate with VG model,
3. VG3D for the fully resolved VGs on the 3D flat plate.

Furthermore valid throughout this paper, the FP2D and VG2D computations were carried out using a differential Reynolds stress model (DRSM) as a turbulence model with pressure-strain rate model corresponding to the Wallin & Johansson explicit algebraic Reynolds stress model (EARSM) with curvature correction (Wallin and Johansson (2002)). This WJ-DRSM was also linked with the Hellsten k-ω turbulence model (Hellsten (2005)). The VG3D computations, instead, were carried out by means of the WJ-EARSM turbulence model without curvature correction (Wallin and Johansson (2000)), again linked with the Hellsten k-ω turbulence model. This was done since the VG model was formulated for DRSM turbulence models and because the VG3D case solely resolved the vortex structures in the flow itself, not in the turbulence description as for the VG model. All computations were carried out with the Edge CFD code (Eliasson (2002)) and the lift slope factor K in Eq. 1 was set to 1.8π for all VG model computations, i.e. 10 % lower than for the thin airfoil theory.

Boundary conditions for APG flow

For all computational cases, a 0.25 m high and 7.25 m long rectangular computational domain was created, which included a 0.25 m long symmetry plane in front of the flat plate, giving a total length of $l_{plate} = 7.00$ m for the wall boundary. The height of the domain was therefore 0.05 m smaller than in experiments, see Fig. 2. For both domains, the upper boundary was divided into two parts: first, a no-slip wall boundary part from the inflow boundary at x = -0.25 m up to x = 1.25 m that forced the flow in the x-direction as in the experiments. Second, another boundary from x = 1.25 m up to the outflow position at 7.00 m with weak characteristic boundary conditions where an APG and a following favorable pressure gradient (FPG) distribution was set in order to generate the corresponding wall pressure distribution from experiments on the flat plate in computations.

Table 2: Separation region length and its location from flat plate experiments for case II given in first row, taken from Lögdberg et al. (2009), and computational results from the FP2D computations given in remaining rows.

Case	x_{sep} [m]	x_{att} [m]	l_{sep} [m]
Exps II	2.24	2.85	0.61
EARSM	1.87	2.62	0.75
DRSM	-	-	-
$DRSM_m$	1.91	2.42	0.51

Both for the 2D and the 3D grid, the value for the first grid point at the wall was set to y = 10^{-5} m throughout the domain, giving values of $y^+ = \mathcal{O}(1)$. As mentioned earlier, the computational domain in 3D fully resolved the VGs, assuming a no-slip condition not only on the flat plate but also on the VG blades. Furthermore, symmetry conditions were applied on its xy-boundary planes so that the computational domain could be reduced to including only one VG blade, therefore leading to a 3D grid depth of one half VG pair distance D/2 = 0.075 m (see table 1 and Fig. 1). The computational mesh was generally kept fine in the vicinity of the VGs by means of an O-grid topology.

The free stream velocity and the temperature at the inlet were set according to U_∞ = 26.46 m/s and 20°C, respectively. The pressure distribution on the flat plate from experiments was given between x = 1.15 m - 2.95 m, see also Fig. 3, and therefore did not cover the whole x-coordinate range that was needed for the computations. Therefore, the given wall pressure distribution was mirrored at its peak value at $x_{p_{wall,max}}$ = 2.95 m and a constant continuous pressure was imposed for x $\geq$ 4.75 m down to the domain outlet.

Since early FP2D test runs did not succeed in producing the desired separation bubble on the flat plate, the APG distribution on the upper boundary was slightly changed in peak strength while keeping the same shape as in Fig. 3. FP2D computations with the WJ-EARSM turbulence model resulted in a separated region, see table 2 but the same boundary conditions did not lead to any separation at all for FP2D DRSM computations. In order to achieve a separated region with such boundary conditions, it was decided to adjust the α_1 coefficent in the ω equation of the turbulence model which led to a change in value for α_1 from 0.518 to 0.61. This rather ad-hoc way can be justified by the fact that the main focus of this investigation was primarly the VG model's streamwise position variation and the differences in results. By adjusting the α_1 value, a similar separation bubble as in experiments could be created even with the DRSM turbulence model, yet positioned ca. 0.30 m further upstream than in experiments. Nevertheless, the length of the separated region could be proved to be akin to experiments, see also $DRSM_m$ in table 2.

RESULTS

This chapter presents the results of the FP2D, the VG2D, and the VG3D computations. A baseline case was set and, in addition, a VG model plane position variation was carried out whereas the VG3D computations were only carried out for the baseline case. Both for the baseline case and for the position variation, skin friction and wall pressure coefficient plots are presented in the subsequent chapters. All figures include FP2D, VG2D, and VG3D results. Experimental results without separation control devices, similar to Fig. 3 are also included for the wall pressure coefficient distribution figures.

Baseline case

The same geometrical parameter set-up as in the experiments was used for the baseline cases with flow control. Thus, the 3D resolved VG geometry and the VG model input paramters were identical to the data in table 1. The TE of the fully resolved VGs and of the VG model plane were consequently positioned at $x_{VG_{TE}}$ = 1.54 m downstream of the flat plate LE.

The APG and the FPG in the experiments (see Fig. 2) were established through the curved upper wind tunnel wall plus the suction system. In the computations, this was arranged through a predescribed pressure distribution at the upper boundary of the computational domain, as described in the previous chapter.

Figure 4 shows the wall pressure coefficient distribution of both, the uncontrolled cases and the controlled cases. All curves were normalized with corresponding pressures at x = 1.15 m. The experimental results show a very steep increase in wall pressure very near the location $x_{APG_{start}}$ = 1.25 m. The constant part of dc_p/dx lasts up until ca. x = 2.00 m from where on the pressure coefficient flattens and rather quickly develops another constant gradient region from x = 2.25 m up to ca. $x_{APG_{end}}$ = 2.95 m. This region can be identified as the separated region, compare also with table 2.

The FP2D case gives a rather similar wall pressure distribution, giving a slightly steeper pressure increase and an earlier separation region at x = 1.91 m. The peak pressure value is not located in the separation bubble but at ca. x = 3.10 m right behind the end of the APG region. The pressure coefficient decreases from $c_{p,max_{FP2D}}$ = 0.603 down to $c_{p,out_{FP2D}}$ = -0.142 at the outlet, giving a $\Delta c_{p,FP2D}$ = $c_{p,max_{FP2D}}$ - $c_{p,out_{FP2D}}$ = 0.745. The wall skin friction in Fig. 5 shows additional information of the separation bubble location and the general distribution along the ZPG, APG and FPG sections. As expected, c_f decreases quickly close to the LE and starts to fall even quicker when the APG is forced on the flow at x = 1.25 m. The skin friction coefficient drops below zero between x = 1.91 m - 2.42 m, describing the exact location of the backflow region close to the wall. The increase in skin friction is a direct consequence of the decrease in pressure gradient at the wall and reaches a peak where the FPG ends.

The VG2D results instead show how the VG model changes the pressure distribution along the flat plate, see Fig. 4. It can be clearly seen that the pressure increase is slightly weaker than for FP2D and that a continuous increase up to $c_{p,max_{VG2D}}$ = 0.680 throughout the whole APG range happens. This pressure coefficient rise corresponds to $\Delta c_{p,max}$ = $c_{p,max_{VG2D}}$ - $c_{p,max_{FP2D}}$ = 0.077 compared to the uncontrolled case. The separation region is not present any more which can be observed in Fig. 5 where the skin friction coefficient does not cross the 0-line anymore. The pressure coefficient at the domain's outlet for VG2D is $c_{p,out_{VG2D}}$ = -0.084 and is increased by 0.058 compared to the uncontrolled case. $\Delta c_{p,VG2D}$ = $c_{p,max_{VG2D}}$ - $c_{p,out_{VG2D}}$ = 0.764, giving a larger pressure coefficient difference between the maximum and minimum wall pressure for the VG2D case, yet having less total pressure losses, compared to FP2D. This successfully proves the capability of the VG model to prevent separation for this APG flow case.

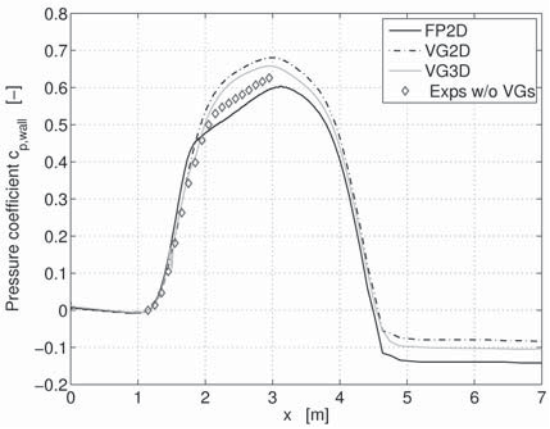

Figure 4: Wall pressure coefficient distributions for FP2D, VG2D, VG3D, and experiments.

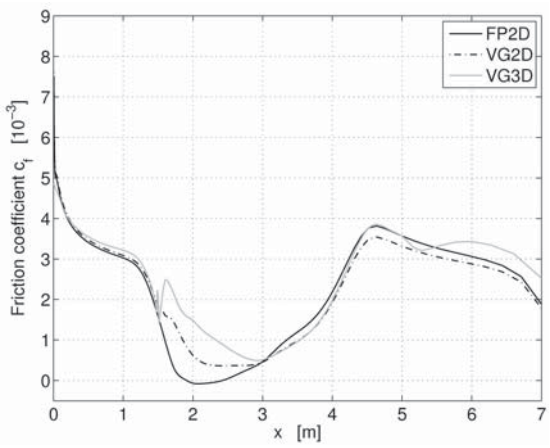

Figure 5: Local skin friction coefficient distributions for FP2D, VG2D, and VG3D.

Spanwise averaged fully resolved VG3D results are also presented in figures 4 and 5. It can be seen that the wall pressure distribution is generally slightly lower, yet very similar to the VG2D results as described in the previous paragraph. The pressure loss across the VGs can be detected at around x = 1.50 m and the first half of the VG3D curve is situated between the VG2D and the experimental curves. The pressure recovery at the outlet is with $c_{p,out_{VG3D}}$ = -0.105 not as high as for the VG2D computations ($c_{p,out_{VG2D}}$ = -0.084) but the total pressure coefficient difference between the maximum ($c_{p,max_{VG3D}}$ = 0.659) and the outlet wall pressure coefficient exactly matches the VG2D value, $\Delta c_{p,VG3D}$ = $c_{p,max_{VG3D}}$ - $c_{p,out_{VG3D}}$ = 0.764. The VG2D computations seem to be therefore well in agreement with the VG3D computations. The skin friction coefficient plot shows an enhanced distribution in the APG section compared to the uncontrolled FP2D results. Later on in the FPG section, the curve collapses with the VG2D curve but diverges as it approaches the downstream constant pressure section. Here the VG3D curve describes a rather different curve than for the 2D computations. This is possibly the result of the resolved vortex structures that break down as the FPG section ends. The vortex energy could then be transferred into turbulent energy that in turn influences the local skin friction distribution. This difference in skin friction must be investigated in more detail in a future study.

VG model plane variation

Here, four chosen streamwise positions for the VG model plane are presented: $x_{VG_{mod}}$ = 1.25, 1.40, 1.54, and 1.70 m, giving approximately equidistant streamwise distances. Also included in the figures are spanwise averaged results from VG3D and experimental results without separation control for the wall pressure plots.

Figure 6 presents the wall pressure coefficient distributions along the flat plate. Here, the tendency of a higher pressure increase in the APG region as well as a lower total pressure loss at the outlet are clearly visible the more upstream the VG model is placed. This results from the fact that the more upstream the VG model is placed, the higher is the streamwise velocity around the VG model. Therefore, stronger vortices are generated by the VG model that in turn have a stronger effect on the flow than vortices that are generated further downstream. Further downstream at $x_{VG_{mod}}$ = 1.70 m, the wall pressure and the skin friction coefficient distribution in figures 6 and 7 are more similar to the FP2D case, compare with previous figures 4 and 5. Here, the separation bubble is still present because the boundary layer is already so much decelerated that only very weak vortices evolve from this streamwise position, having a lower positive effect on the separation. The efficiency and the effectiveness of the applied separation control devices changes depending on the actual VG model postion, giving lower total pressure losses the more upstream the VG model is placed, i.e. within a smaller boundary layer thickness. The trend that a large distance of the VG model to a separation region is always favorable cannot be proven because it might be the case that far upstream generated vortices encounter sooner breakdown or strong diffusion which weakens the positive influence on the mean flow before they actually reach the interesting region. This should be further investigated in a subsequent study.

The skin friction coefficient results in Fig. 7 again show how the VG model position affects the flow and the separation region. The effect of the VG model far upstream results in a distinct peak of the skin friction coefficient, similar to the VG3D peak around the resolved VG TE. The local flow is generally enhanced for all VG model locations except for $x_{VG_{mod}}$ = 1.70 m, as mentioned above. In the FPG section and the downstream constant pressure section, all favorable VG model computations more or less collapse, describing similar flow fields downstream the APG region. Again, it is not sure if a further increase of the distance between the VG model plane and the separation region leads to even better results in the region of interest. On the other hand, it is important to recall that higher velocities around the VG model also induce higher parasitic drag to the mean flow. This is a trade-off situation and needs to be considered when this VG model is used within engineering applications.

CONCLUSIONS

This investigation of a APG flat plate boundary layer has shown the capabilities of a statistical 2D VG model to mimic the effects of VG arrays in APG flow by means of introducing additional statistical vortex stresses to the governing equations.

Wall pressure and skin friction coefficient distribution plots have shown that the VG2D model computations successfully improve the flow by means of preventing the initial separation on the clean flat plate. This can be seen by comparing corresponding flat plate computations as well as experimental plots with the VG model computation plots in

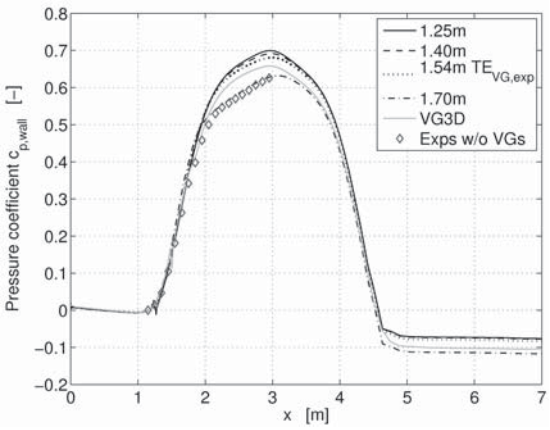

Figure 6: Wall pressure coefficient distributions for VG model streamwise position variation, VG3D, and experiments.

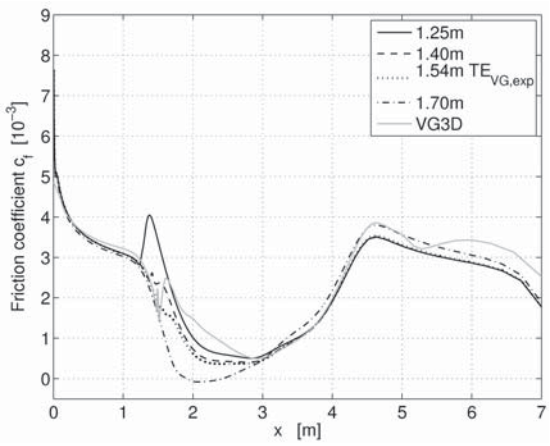

Figure 7: Local skin friction distributions for VG model streamwise position variation, and VG3D.

Fig. 4 and 5. The lower total pressure losses at the outlet plane of the controlled cases in the wall pressure plots indicate how the total flow losses are decreased using controlling devices, either the VG model or resolved structures. The actual differences in the VG2D and resolved VG3D computations are expected since the VG model describes the vortex structures from a 2D vortex model in a turbulent statistical way rather than resolving their structures as it is the case for the 3D computations. Therefore, velocity and also skin friction results are likely to be different to experiments and results from resolved computations. Nevertheless, it is important to point out that the goal, the overall separation prevention, has been successfully shown for the VG model.

A VG model plane variation, compare figures 6 and 7, shows how the streamwise postion of the VG model influences the mean flow results of the wall pressure and skin friction coefficient distributions. The differences in the position variation can be observed in terms of the pressure peak variation and the total pressure loss differences at the domain outlet in Fig. 6. The trends and tendencies from the parameter variation show that the VG model should be placed a certain distance upstream of the flow separation in order to be able to generate the required second order turbulent statistics that have the desired preventative impact on the mean flow.

This investigation has shown that the statistical VG model approach is very promising for an application in APG flow and has the advantage of not being more computational expensive than solving RANS equations without modeled VGs, leading to much faster results than with conventional methods such as fully or partly resolved VGs.

ACKNOWLEDGMENTS

The experiments were carried out within a cooperative research program between KTH Stockholm and Scania AB, Sweden, and the provision of results is grateful acknowledged.

REFERENCES

Anderson, J. D., 1991, *Fundamentals of Aerodynamics*, McGraw-Hill, 2nd Ed., 772 pages.

Angele, K., 2003, "Experimental studies of turbulent boundary layer separation and control", Ph.D. thesis, Department of Mechanics, KTH Stockholm, Sweden.

Dengel, P., and Fernholz, H. H., 1990, "An experimental investigation of an incompressible turbulent boundary layer in the vicinity of separation", *Journal of Fluid Mechanics*, Vol. 212, pp. 615-636.

Eliasson, P., 2002, "EDGE, a Navier-Stokes Solver for Unstructured Grids", *Proceedings to Finite Volumes for Complex Applications III*, Hemre Penton Science London, pp. 527-534.

Glauert, H., 1926, *The Elements of Aerofoil and Airscrew Theory"*, Cambridge University Press, London, UK, 1st ed., 228 pages.

Hellsten, A., 2005, "New Advanced k-ω Turbulence Model for High-Lift Aerodynamics", *AIAA Journal*, Vol. 43, No. 9, pp. 1857-1869.

Lin, J. C., 2002, "Review of Research on Low-Profile Vortex Generators to Control Boundary-Layer Separation", *Progress in Aerospace Sciences*, Vol. 38, pp. 389-420.

Lindgren, B., and Johansson, A. V., 2004, "Evaluation of a new wind tunnel with expanding corners", *Exp. Fluids*, Vol. 36, pp. 197-203.

Lögdberg, O., Fransson, J. H. M., and Alfredsson, P.H., 2009, "Streamwise Evolution of Longitudinal Vortices in a Turbulent Boundary Layer", *Journal of Fluid Mechanics*, Vol. 623, pp. 27-58.

Törnblom, O., and Johansson, A. V., 2008, "A Reynolds Stress Closure Description of Separation Control With Vortex Generators in a Plane Asymmetric Diffuser", *Physics of Fluids*, Vol. 19, No. 115108.

von Stillfried, F., Wallin, S., and Johansson, A. V., 2009, "Statistical modeling of the influence of turbulent flow separation control devices", *AIAA conference paper*, 47th AIAA Aerospace Sciences Meeting, Orlando, FL, USA, AIAA 2009-2501.

Wallin, S., and Johansson, A. V., 2000, "An Explicit Algebraic Reynolds Stress Model for Incompressible and Compressible Turbulent Flows", *Journal of Fluid Mechanics*, Vol. 403, pp. 89-132.

Wallin, S., and Johansson, A. V., 2002, "Modelling Streamline Curvature Effects in Explicit Algebraic Reynolds Stress Turbulence Models", *International Journal of Heat and Fluid Flow*, Vol. 23, No. 5, pp. 721-730.

Wendt, B., 2001, "Initial Circulation and Peak Vorticity Behavior of Vortices Shed From Airfoil Vortex Generators", NASA/CR-2001-211144l.